Investigation of electrochromic band-shifts in the Soret region induced by the formation of $Tyr_D^{\bullet}$, $Tyr_Z^{\bullet}$, and $Q_A^{\bullet -}$ in Photosystem II.

Alain Boussac*[1], Takumi Noguchi[2], A. William Rutherford[3], Julien Sellés[4], Miwa Sugiura[5], Stefania Viola[6].

The authors are given in alphabetic order

*Corresponding author

[1]Institut de Biologie Intégrative de la Cellule, UMR9198, CEA Saclay, 91191 Gif-Sur-Yvette, France. alain.boussac@laposte.net

[2]Department of Physics, Graduate School of Science, Nagoya University, Furo-cho, Chikusa-ku, Nagoya 464-8602, Japan. tnoguchi@bio.phys.nagoya-u.ac.jp

[3]Department of Life Sciences, Imperial College, SW7 2AZ London, UK. a.rutherford@imperial.ac.uk

[4]Institut de Biologie Physico-Chimique, UMR CNRS 7141 and Sorbonne Université, 13 rue Pierre et Marie Curie, 75005 Paris, France. selles@ibpc.fr

[5]Proteo-Science Research Center, and Department of Chemistry, Graduate School of Science and Technology, Ehime University, Bunkyo-cho, Matsuyama, Ehime 790-8577, Japan. miwa.sugiura@ehime-u.ac.jp

[6]Institute of Biosciences and Biotechnologies of Aix-Marseille – UMR7265, Saint-Paul-Lez-Durance, France. stefania.viola@cea.fr

ORCID numbers:

Alain Boussac: 0000-0002-3441-3861

Takumi Noguchi: 0000-0002-3281-6827

A. William Rutherford: 0000-0002-3124-154X

Julien Sellés: 0000-0001-9262-8257

Miwa Sugiura: 0000-0002-4232-5941

Stefania Viola: 0000-0003-0773-8158

Abstract

The effects of $Tyr_D^{\bullet}$, $Tyr_Z^{\bullet}$, and $Q_A^{\bullet-}$ radical formation on the absorption spectrum in the Soret region were studied in Mn-depleted Photosystem II at pH 8.6 (in order to be in the Tyr_D state after dark adaptation). Flash-induced difference spectra were recorded in several PSII samples from: *i*) *Thermosynechococcus vestitus* (formerly *T. elongatus*), *ii*) *Synechocystis sp.* PCC 6803, *iii*) *Chroococcidiopsis thermalis* PCC 7203 grown under far-red light, and *iv*) *Acaryochloris marina*. In the case of *T. vestitus*, mutants D1/H198Q, D1/T1789H, D2/I178H, and D2/Y160F, with PsbA1/Q130 instead of PsbA3/E130, were also studied for possible contributions from P_{D1}, Chl_{D1}, Chl_{D2}, and Phe_{D1}, respectively. For a possible contribution from P_{D2}, the D2/H197A mutant was studied in *S. 6803*. While P_{D1} is clearly the species whose spectrum is blue-shifted by ~3nm in the presence of $Q_A^{\bullet-}$, as has already been well documented in the literature, the species whose spectra shift upon the formation of $Tyr_D^{\bullet}$ and $Tyr_Z^{\bullet}$ remain to be clearly identified, as they appear different from P_{D1}, P_{D2}, Phe_{D1}, Chl_{D1}, and Chl_{D2}, as concluded by the lack of different light-induced difference spectra in the mutants listed above. Although we cannot rule out a weak effect, considering the accuracy of the experiments, it is proposed that other pigments, such as antenna Chl and/or Car, near the reaction center are involved. Additionally, it is shown that: *i*) there is no proton release into the bulk upon the oxidation of Tyr_D at pH 8.6, and *ii*) the rearrangement of the electrostatic environment of the pigments involved in the light-induced difference spectra in the samples studied, upon the formation of $Tyr_D^{\bullet}$, $Tyr_Z^{\bullet}$, and $Q_A^{\bullet-}$, likely occurs differently from both a kinetic and structural perspective.

Introduction

Oxygenic photosynthesis in cyanobacteria, algae, and higher plants converts solar energy into the chemical bonds of sugars and dioxygen. Photosystem II (PSII) begins this process by splitting water to obtain electrons in the form of reduced quinones, while generating a proton gradient and releasing O□. The mature PSII binds 35 chlorophyll *a* (Chl-*a*), 2 pheophytins (Phe-*a*), 1 membrane b-type cytochrome, 1 extrinsic c-type cytochrome (in cyanobacteria and red algae), 1 non-heme iron, 2 plastoquinones (Q_A and Q_B), the Mn□CaO□ cluster, 2 Cl□, 12 carotenoids, and 25 lipids [1,2]. In the cyanobacterium *Synechocystis sp.* PCC 6803, a fourth extrinsic subunit, PsbQ, has also been found in addition to PsbV, PsbO, and PsbU [3].

Among the 35 Chl-a molecules, 31 are antenna Chl's. When one is excited, the excitation energy is transferred to other chlorophylls until it reaches the key pigments in the photochemical reaction center [3]: 4 Chl-*a* molecules, P_{D1}, P_{D2}, Chl_{D1}, Chl_{D2}, and 2 Phe-*a* molecules, Phe_{D1} and Phe_{D2}. A few picoseconds after the formation of the excited $^*Chl_{D1}$, charge separation occurs, ultimately resulting in the formation of the $Chl_{D1}^{\bullet+}Phe_{D1}^{\bullet-}$ and then $P_{D1}^{\bullet+}Phe_{D1}^{\bullet-}$ radical pair states [5,6]. The formation of the $Chl_{D1}^{\bullet+}Phe_{D1}^{\bullet-}$ radical pair was recently defined as a fast pathway (short-range charge separation) in contrast with a slow pathway where $P_{D1}P_{D2}$ acts as the initial donor (long-range charge separation), which would result directly in the formation of the $P_{D1}^{\bullet+}Phe_{D1}^{\bullet-}$ radical pair [7].

After this charge separation, $P_{D1}^{\bullet+}$ oxidizes Tyr_Z, the Tyr161 of the D1 polypeptide, which is then reduced by the Mn□CaO□ cluster. The electron on $Phe_{D1}^{\bullet-}$ is then transferred to Q_A, the primary quinone electron acceptor, and then to Q_B, the secondary quinone electron acceptor. While Q_A can only be singly reduced under normal conditions, Q_B accepts two electrons and two protons before leaving its binding site and being replaced by an oxidized Q_B molecule from the membrane plastoquinone pool. For a non-exhaustive list of recent reviews on PSII function, see for example [8–12]. The Mn□CaO□ cluster, oxidized by the $Tyr_Z^{\bullet}$ radical formed after each charge separation, cycles through five redox states denoted S_n, where n represents the number of stored oxidizing equivalents. When the S_4-state is formed, two water molecules bound to the cluster are oxidized, O□ is released, and the S_0-state is reformed [13,14].

Formation of the $Q_A^{\bullet-}$ species is known to induce spectral changes in Phe_{D1} in the Qx region around 550 nm [15-17], and in P_{D1} in the Qy region between 650 and 700 nm [18,19]. These electrochromic responses have been extensively studied both experimentally and theoretically

[18,19]. For example, it has been observed that in the presence of $Q_A^{\bullet-}$, the blue shift of the Qy band of Chl_{D1}, typically seen at ~680 nm, was replaced by one at ~727 nm in far read light PSII (FRL-PSII), indicating that the Chl-*a* acting as Chl_{D1} was replaced by a FRL chlorophyll (likely a Chl-*d*) [20]. The Soret band of P_{D1} is also sensitive to the formation of $Q_A^{\bullet-}$ and to the charge in and around the Mn□CaO□ cluster [21,22]. That said, spectral changes in the blue region are far less well-studied than the Qx and Qy bands, although see [18] for further discussion. For this reason, we report here an initial characterization of the spectral changes between 400 and 460 nm induced by the formation of the $Tyr_D^{\bullet}$, $Tyr_Z^{\bullet}$, and $Q_A^{\bullet-}$ radicals. In order to achieve the highest proportion of centers with a reduced Tyr_D after dark adaptation, and to avoid contributions from the Mn□CaO□ cluster, the experiments were performed at pH 8.6 in several Mn-depleted PSII preparations [23].

Materials and Methods

The PSII samples used were: *i*) the PsbA3-PSII [24], the PsbA3/H198Q mutant [25], the PsbA3/T179H mutant [26], the Tyr_D-less mutant (with D1 = PsbA1) [27], and the D2/I178H mutant (with D1 = PsbA3) [28], all purified from *Thermosynechococcus vestitus*; *ii*) the FRL-PSII from *Chroococcidiopsis thermalis* [20,29], with 4 Chl-*f* and 1 Chl-*d*; *iii*) the wild-type and D2/H197A mutant from *Synechocystis* 6803 [30]; and *iv*) PSII from *Acaryochloris marina* [29], with 34 Chl-*d* and 1 Chl-*a* at the P_{D1} position [31].

The samples were Mn-depleted by adding approximately 10 mM NH□OH (from a 1 M stock at pH 6.5) and 1 mM EDTA. The hydroxylamine was then removed by washing the PSII samples through cycles of dilution in 1 M betaine, 15 mM CaCl□, 15 mM MgCl□, 100 mM Tris, 100 µM EDTA, pH 8.6 (adjusted with HCl), followed by concentration using Amicon Ultra-15 centrifugal filter units (cut-off 100 kDa) until the estimated residual NH□OH concentration was lower than 0.1 µM in the concentrated PSII samples before the final dilution. In the final dilution step, the PSII samples were suspended in 1 M betaine, 15 mM CaCl□, 15 mM MgCl□, 100 mM Tris, pH 8.6. For the experiment reported in Fig. 8, the Tris buffer was replaced with Mes buffer at pH 6.5.

For the measurements with the dye thymol blue, the Mn-depleted Tyr_D-less PSII at pH 8.6 was washed through cycles of dilution in 100 mM NaCl, 15 mM CaCl□, and 15 mM MgCl□, followed by concentration using Amicon Ultra-15 centrifugal filter units (cut-off 100 kDa), until the estimated residual Tris concentration was lower than 1 µM in the concentrated PSII samples before the final dilution. After dark adaptation for 3 to 4 hours at room

temperature, 150 µM thymol blue and 100 µM PPBQ (in dimethyl sulfoxide) were added. During the measurement, the sample was continuously bubbled with ALPHAGAZ 2 Argon from Air Liquide, in which the CO_2 contamination is ≤ 0.1 ppm. This bubbling was performed to minimize drift in the baseline (*i.e.*, in the pH) due to the solubilization of atmospheric CO_2.

Time-resolved absorption changes were measured with a lab-built spectrophotometer [32], modified as described in detail in [33]. The chlorophyll concentration of the samples was approximately 25 µg of Chl mL^{-1}.

Results and Discussion

Panel A in Fig. 1 shows the ΔI/I recorded at 432 nm in Mn-depleted PsbA3-PSII at pH 8.6, illuminated by 10 saturating flashes (spaced 2 s apart) in the presence of the electron acceptor PPBQ. The sample was dark-adapted for 3 to 4 hours at room temperature before the flash illumination. Panel B shows a zoom of the data recorded after the first 4 flashes. In this experiment, the first weak, non-actinic detector flash was given 200 µs after each actinic flash. The second weak, non-actinic detector flash was given 10 ms after each actinic flash. Then, 20 weak, non-actinic detector flashes (spaced 100 ms apart) were given after each of the 10 actinic flashes.

At pH 8.6, and after a long dark-adaptation, Tyr_D is reduced in the great majority of the centers. Under these conditions, the first actinic flash oxidizes either Tyr_D or Tyr_Z in almost equal proportions [23]. The non-decaying ΔI/I recorded 2 s after the first flash (black vertical arrow in Panel B of Fig. 1) is a consequence of $Tyr_D^{\bullet}$ formation alone, since 2 s after the flash, $Tyr_Z^{\bullet}$ and $Q_A^{\bullet-}$ are no longer present. Always after the first flash, the yellow vertical arrow (the 200 µs-*minus*-10 ms difference) corresponds to a mixture of the $Tyr_D^{\bullet}Q_A^{\bullet-}$-*minus*-$Tyr_D^{\bullet}Q_A$ and $Tyr_Z^{\bullet}Q_A^{\bullet-}$-*minus*-$Tyr_Z^{\bullet}Q_A$ differences. In other words, it is a mix of the $Q_A^{\bullet-}$-*minus*-Q_A difference in the presence of either $Tyr_D^{\bullet}$ or $Tyr_Z^{\bullet}$. After the 4th flash, when $Tyr_D^{\bullet}$ is formed in virtually all centers, the flash illumination only induces the formation of the $Tyr_Z^{\bullet}Q_A^{\bullet-}$ state, and the slow decay in the second (s) time range corresponds to the decay of $Tyr_Z^{\bullet}$. Consequently, the red vertical arrow (the 200 µs-*minus*-10 ms difference) corresponds to the $Tyr_Z^{\bullet}Q_A^{\bullet-}$-*minus*-$Tyr_Z^{\bullet}Q_A$ difference, in other words, the $Q_A^{\bullet-}$-*minus*-Q_A difference in the presence of $Tyr_Z^{\bullet}$ and $Tyr_D^{\bullet}$. This differs from the first flash, where the $Q_A^{\bullet-}$-*minus*-Q_A difference was measured in the presence of only one of the two tyrosyl radicals, either $Tyr_Z^{\bullet}$ or $Tyr_D^{\bullet}$. Always after the 4th flash, the violet vertical arrow in Panel B of Fig. 1 is the ΔI/I

200 µs after flash n *minus* 2 s after flash n-1. It corresponds to the $Tyr_Z^{\bullet}Q_A^{\bullet-}$-*minus*-$Tyr_ZQ_A$ difference. Finally, the green vertical arrow (300 ms-*minus*-2 s) in Panel B of Fig. 1 corresponds to $Tyr_Z^{\bullet}$-*minus*-Tyr_Z difference alone (in the presence of $Tyr_D^{\bullet}$).

The lower ΔI/I amplitude observed 200 µs after the first flash, compared with subsequent flashes, was most likely due to centers where non-heme iron was oxidized prior to flash illumination. Indeed, in these centers, the electron transfer from $Q_A^{\bullet-}$ to Fe^{3+} is completed well before 200 µs [34,35].

The experiment presented in Fig. 1 was repeated for wavelengths ranging from 401 nm to 457 nm. To improve the signal-to-noise ratio, except for the data corresponding to the first flash, the spectra were averaged from the 6th to the 10th flashes. Fig. 2 shows the five spectra corresponding to the electrochromic responses defined in Panel B of Fig. 1, using the same color code.

The spectrum in red, corresponding to the $Q_A^{\bullet-}$-*minus*-Q_A difference in the presence of both $Tyr_Z^{\bullet}$ and $Tyr_D^{\bullet}$, may raise some questions. Indeed, it appears somewhat similar to the difference spectrum $[P_{D1}P_{D2}]^{\bullet+}Q_A^{\bullet-}$-*minus*-$[P_{D1}P_{D2}]Q_A$ recorded 20 ns after a flash [36]; see also [18]. The amplitude of the $[P_{D1}P_{D2}]^{\bullet+}Q_A^{\bullet-}$ spectrum at 432 nm, recorded 20 ns after the flash under the same setup and with a similar sample, was ~0.016 ΔI/I [36], approximately 11 times larger than the red spectrum observed here. The presence of ~10% $[P_{D1}P_{D2}]^{\bullet+}$ at 200 µs after the flash could thus account for the ΔI/I signal recorded at 432 nm.

However, attributing the species responsible for the slow decay in the 432-446 nm range is challenging [36]. See, however, the data at 820 nm [37]. Specifically, the measured decay corresponds to the $[P_{D1}P_{D2}]^{\bullet+}Q_A^{\bullet-}$ spectrum, which necessarily also includes spectral contributions arising from $Q_A^{\bullet-}$ formation. Most likely, these contributions are responsible for the phases observed in the hundreds of microseconds time range, which correspond to the electron transfer from $Q_A^{\bullet-}$ to Q_B. (There is no transfer to $Q_B^{\bullet-}$, which is not present due to the addition of PPBQ, *e.g.*, [38].)

Additionally, the red spectrum in Fig. 2 closely resembles, both in shape and amplitude, the electrochromic shift induced by $Q_A^{\bullet-}$ formation, attributed to a change in P_{D1} absorption under conditions where P_{680}^{+} is excluded [22].

The $Q_A^{\bullet-}$-*minus*-Q_A difference spectrum after the first flash (orange spectrum) shows a 2 nm blue shift compared to the red spectrum, from ~434 nm to ~432 nm. This indicates that the presence of both tyrosyl radicals shifts the $Q_A^{\bullet-}$-*minus*-Q_A difference spectrum to the red compared to the condition with $Tyr_D^{\bullet}$ alone. As explained earlier, after the first flash, there is a mixture of two difference spectra because $Tyr_Z^{\bullet}$ and $Tyr_D^{\bullet}$ are formed in approximately

equal proportions [23]. This implies that the difference between the first flash spectrum and the average spectrum from the 6th to the 10th flashes would have been larger if $Tyr_D^{\bullet}Q_A^{\bullet-}$ had been formed exclusively after the first flash.

It is also noteworthy that the $[P_{D1}P_{D2}]^{\bullet+}$ spectrum measured 20 ns after a flash shows a dip at the same wavelength (~432 nm) after both the first and subsequent flashes [36]. This provides additional evidence against attributing the orange and red spectra to $[P_{D1}P_{D2}]^{\bullet+}$.

While the pigment whose absorption is modified by $Q_A^{\bullet-}$ formation has been clearly identified as P_{D1} (*e.g.*, [21,22]), the pigment(s) affected by the formation of $Tyr_Z^{\bullet}$ and $Tyr_D^{\bullet}$ remain unidentified. This is the focus of the experiments reported below, which use PSII mutants and PSII from different species.

Panel A of Fig. 3 shows the ΔI/I signal recorded at 432 nm in Mn-depleted, Tyr_D-less PSII [27] at pH 8.6, illuminated with 10 saturating flashes (spaced 2 seconds apart) in the presence of the electron acceptor PPBQ. Despite the absence of Tyr_D in this PSII, the sample was dark-adapted for 3–4 hours at room temperature before flash illumination.

Panel B of Fig. 3 displays the spectra constructed as described in Panel B of Fig. 1. Due to the absence of Tyr_D, $Tyr_Z^{\bullet}$ was formed after the first flash. The black spectrum recorded 2 seconds after the first flash is therefore attributed to the $Tyr_Z^{\bullet}$-*minus*-Tyr_Z difference spectrum (green spectrum).

Two additional observations can be made: *i*) The $Q_A^{\bullet-}$-*minus*-Q_A difference spectrum after the first flash (orange spectrum) is identical to the $Q_A^{\bullet-}$-*minus*-Q_A difference spectrum recorded after subsequent flashes. *ii*) The trough of this spectrum in the presence of $Tyr_Z^{\bullet}$ alone is located at ~433 nm, which is intermediate between the $Q_A^{\bullet-}$-*minus*-Q_A difference spectra observed in the presence of either $Tyr_D^{\bullet}$ alone or both $Tyr_D^{\bullet}$ and $Tyr_Z^{\bullet}$.

This experiment demonstrates that the $Q_A^{\bullet-}$-*minus*-Q_A difference spectrum shows slight variations across three conditions: with $Tyr_D^{\bullet}$ alone, $Tyr_Z^{\bullet}$ alone, or both $Tyr_D^{\bullet}$ and $Tyr_Z^{\bullet}$.

In Mn-depleted PSII at pH 6.5, the oxidation of both Tyr_Z and Tyr_D is coupled to proton release into the bulk [39,40]. In [39], it was proposed that the proton released upon $Tyr_D^{\bullet}$ formation is directly released from the protein rather than being transferred to the neighboring D2-His198, unlike the process during $Tyr_Z^{\bullet}$ formation, where the proton is transferred to the hydrogen-bonded D1-His190.

At pH 8.6, a pH value at which $Tyr_D^{\bullet}$ is unstable in the dark, no information is currently available about the proton release following Tyr_D oxidation. Fig. 4 presents an experiment that tracks proton release into the bulk at pH 8.6, using the dye thymol blue, after

a series of flashes applied to dark-adapted Mn-depleted PsbA3-PSII. At 580 nm, medium acidification results in a decrease in thymol blue absorption.

The sample was illuminated with ten flashes, spaced 2 seconds apart, and the ΔI/I was measured every 100 ms (the first detection occurred 20 µs after the actinic flashes). The black trace represents the raw data. The red curve corresponds to a polynomial fit, and the blue trace is obtained by subtracting the polynomial fit from the black trace. This subtraction was performed to minimize drift in the black trace.

Despite bubbling the PSII suspension with pure argon gas, the drift likely results from the solubilization of trace amounts of atmospheric CO_2.

The first conclusion from the experiment shown in Fig. 4 is that Tyr_D oxidation is not coupled to proton release into the bulk, as evidenced by the absence of a color change in thymol blue after the first flash. This contrasts with the oxidation of Tyr_Z during subsequent flashes, where a proton was released with kinetics not resolved in this experiment. The decay of $Tyr_Z^{\bullet}$ was then coupled to proton uptake by PSII, with kinetics similar to those observed at 432 nm in Fig. 1A. To our knowledge, this is the first measurement of proton release and uptake at pH 8.6 associated with the oxidation of Tyr_D and subsequently Tyr_Z.
The second conclusion is that both Tyr_Z and Tyr_D oxidations have an electrochromic effect on one or more pigments nevertheless the observation that in the case of Tyr_Z oxidation, the proton is released into the medium, whereas in the case of Tyr_D, no proton release occurs.

In the following sections, we present comparisons of the different spectra defined in Panel B of Fig. 1, obtained from Mn-depleted PSII in mutants and PSII with different pigment compositions. These include the D1/H198Q [25], D1/T179H [26], and D2/I178H [28] mutants; FRL-PSII from *C. thermalis*, containing 4 Chl-*f* and 1 Chl-*d* [20]; and PSII from *A. marina*, containing 1 Chl-*a* (PD1) and 34 Chl-*d* [29].

Panel A in Fig. 5 presents the $Tyr_Z^{\bullet}Q_A^{\bullet-}$-*minus*-$Tyr_Z^{\bullet}Q_A$ difference spectra for PsbA3-PSII (black spectrum), D1/H198Q-PSII (red spectrum), D1/T179H-PSII (blue spectrum), and FRL-PSII from *C. thermalis* (green spectrum). As expected, the most significant spectral modification was observed in the D1/H198Q mutant, where the axial ligand of P_{D1} has been altered. In this mutant, the trough was shifted ~3–4 nm to the blue, from 433–434 nm in PsbA3-PSII to 430 nm.

The $Tyr_Z^{\bullet}Q_A^{\bullet-}$-*minus*-$Tyr_Z^{\bullet}Q_A$ difference spectrum in PsbA3-PSII displayed a shoulder at 443–444 nm. This shoulder was not shifted in the D1/H198Q-PSII. However, in FRL-PSII, where Chl_{D1} is likely a Chl-*d*, this shoulder was shifted ~3 nm to the red. This shift was accompanied by a narrowing of the spectrum between 434 nm and 440 nm, confirming

the red shift of a spectral component. In the D1/T179H mutant, where Chl_{D1} is also affected, the shoulder at 443–444 nm also appeared modified, albeit less prominently.

Panel B in Fig. 5 displays the $Tyr_Z^{\bullet}Q_A^{\bullet-}$-*minus*-$Tyr_ZQ_A$ difference spectra for PsbA3-PSII (black spectrum), D1/H198Q-PSII (red spectrum), D1/T179H-PSII (blue spectrum), and FRL-PSII from *C. thermalis* (green spectrum). The shape of these spectra suggests that two pigments absorbing near 430 nm are affected by the formation of $Tyr_Z^{\bullet}Q_A^{-}$, with one pigment exhibiting a blue shift and the other a red shift. The effect of the D1/H198Q mutation indicates that one of these two pigments is clearly P_{D1}. In a previous study conducted on O□-evolving PSII at pH 6.5 [41], we interpreted similar spectra associated with $Tyr_Z^{\bullet}Q_A^{\bullet-}$ formation as arising from a red shift in the Soret band of P_{D1} and a blue shift in the Soret band of Chl_{D1}. Unfortunately, the signal-to-noise ratio of the current spectra, compared with those in [41], is insufficient to confirm or refute the involvement of Chl_{D1} in the $Tyr_Z^{\bullet}Q_A^{\bullet-}$-*minus*-$Tyr_ZQ_A$ difference spectrum under these experimental conditions.

Panel C in Fig. 5 shows the $Tyr_Z^{\bullet}$-*minus*-Tyr_Z difference spectra for PsbA3-PSII (black spectrum), D1/H198Q-PSII (red spectrum), D1/T179H-PSII (blue spectrum), and FRL-PSII from *C. thermalis* (green spectrum). These spectra similarly suggest that more than one pigment absorbing around 430 nm is affected by the formation of $Tyr_Z^{\bullet}$ compared to Tyr_Z. Surprisingly, the spectrum remained unchanged in the D1/H198Q mutant, strongly suggesting that P_{D1} does not undergo an absorption shift upon $Tyr_Z^{\bullet}$ formation.

This finding indicates that pigments other than P_{D1} experience electrochromic shifts in the presence of $Tyr_Z^{\bullet}$. Despite averaging numerous spectra, the signal-to-noise ratio remained insufficient to unambiguously identify these pigments. However, given the spectral range in which the band shifts occur and the lack of effects in the mutants studied, it is plausible that a carotenoid or a chlorophyll other than P_{D1}, Chl_{D1}, or Chl_{D2} may be involved.

Panel D in Fig. 5 presents the $Tyr_D^{\bullet}$-*minus*-Tyr_D difference spectra for PsbA3-PSII (black spectrum), D1/H198Q-PSII (red spectrum), D1/T179H-PSII (blue spectrum), D2/I178H-PSII (orange spectrum) [28], and FRL-PSII from *C. thermalis* (green spectrum). These spectra differ notably from the $Tyr_Z^{\bullet}$-*minus*-Tyr_Z difference spectra. In particular, the $Tyr_D^{\bullet}$-*minus*-Tyr_D difference spectra appear to involve only one pigment, with a clear shift from approximately 430 nm in the presence of Tyr_D to ~446 nm in the presence of $Tyr_D^{\bullet}$. The absence of changes in the difference spectra across the mutants tested suggests that neither P_{D1}, Chl_{D1}, nor Chl_{D2} is involved in this shift.

The situation in FRL-PSII (green spectrum) warrants further commentary. In dark-adapted FRL-PSII, the proportion of centers with a reduced Tyr_D is highly variable, with

virtually no reduction observed in some cases. This variability was confirmed by the amplitude of the $Tyr_D^{\bullet}$ signal in EPR measurements taken before and after illumination (data not shown). This suggests a significant difference compared to other PSII. While the underlying cause of this variability was not further investigated, it implies that the $Tyr_D^{\bullet}$-*minus*-Tyr_D difference spectrum in FRL-PSII may be contaminated by a contribution from the $Tyr_Z^{\bullet}$-*minus*-Tyr_Z difference spectrum.

Despite this, the positive part of the spectrum in the presence of $Tyr_D^{\bullet}$ in FRL-PSII appears to shift to ~449 nm, compared to ~446 nm in the other samples. However, the fact that the pigment's spectrum peaks at 430 nm in the presence of Tyr_D, as observed in other PSII, indicates that the pigment itself does not have an altered spectrum. Instead, this suggests that the electrochromic effect is different in FRL-PSII. This difference likely arises from a modified electrostatic environment in FRL-PSII, as previously mentioned. Such modifications could also explain the distinct stability of $Tyr_D^{\bullet}$ observed in these samples.

One pigment that has not been investigated until now in this report is P_{D2}. To study it, we used PSII from *Synechocystis* 6803, in which the D2/H197A mutant has been constructed [30]. The results are shown in Fig. 6 for the four difference spectra. Surprisingly, even the $Tyr_D^{\bullet}$-*minus*-Tyr_D difference spectrum remained unaffected by the D2/H197A mutation.

The lack of significant effects, except for the P_{D1} mutant D1/H198Q, in the two cases corresponding to the $Tyr_Z^{\bullet}Q_A^{\bullet-}$-*minus*-$Tyr_ZQ_A$ and $Tyr_Z^{\bullet}Q_A^{\bullet-}$-*minus*-$Tyr_Z^{\bullet}Q_A$ difference spectra suggests that, as mentioned above, either pigments other than P_{D2}, Ch_{D1}, and Chl_{D2} are affected, or the spectral changes are too weak given the signal-to-noise ratio of the experiments. One way to confirm this hypothesis is to investigate what happens in the PSII of *A. marina* with 34 Chl-*d* molecules and one Chl-*a*.

It was reported that the $P_{680}^{\bullet+}Q_A^{\bullet-}$-*minus*-$P_{680}Q_A$ difference spectrum at 77 K was identical to that in *T. elongatus* [31], which led the authors to confirm that P_{D1} was the Chl-*a*. Here, we examined the $Tyr_D^{\bullet}$-*minus*-Tyr_D and $Tyr_Z^{\bullet}$-*minus*-Tyr_Z difference spectra. In *A. marina*, unlike in *T. vestitus*, $Tyr_D^{\bullet}$ is not stable in the dark at pH 6.5, which led us to perform the difference spectra at pH 6.5. Of course, it would have been preferable to record them at pH 8.6, but, unfortunately, for a number of reasons beyond our control, we could not do so.

Fig. 7 shows the $Tyr_D^{\bullet}$-*minus*-Tyr_D (Panel A) and $Tyr_Z^{\bullet}$-*minus*-Tyr_Z (Panel B) difference spectra at pH 6.5, in FRL-PSII from *C. thermalis* (black spectra) and in PSII from *A. marina* (red spectra). As expected, $Tyr_D^{\bullet}$ appeared stable at pH 6.5 in *C. thermalis*, with a $Tyr_D^{\bullet}$-*minus*-Tyr_D difference spectrum completely flat in this PSII at this pH. In contrast, in *A. marina*, there was a large $Tyr_D^{\bullet}$-*minus*-Tyr_D difference spectrum. One species whose

spectrum is modified by the oxidation of Tyr_D absorbed at ~455 nm. This supports the hypothesis that this species is a Chl-*d*. It is tempting to propose that this Chl-*d* has an absorption shifted to ~470 nm in the presence of $Tyr_D^{\bullet}$. However, the origin of the positive feature at ~422 nm is less clear. For the $Tyr_Z^{\bullet}$-*minus*-Tyr_Z difference spectra, the situation is even less clear-cut. While the possible presence of two spectral shifts in *A. marina* may be due to the doubling of the Soret band on either side of the Soret band for Chl-*a*, the differences between pH 6.5 and pH 8.6 in the case of *C. thermalis* remain to be understood.

Panel B in Fig. 1 shows that between 10 ms and 500 ms, a change in the ΔI/I occurred in the opposite direction when compared to the decay of $Tyr_Z^{\bullet}$. Panel A in Fig. 8 shows an average of the ΔI/I from the 6th to the 10th flash in PsbA3-PSII from *T. vestitus* (black points), D1/H198Q-PSII (red points), and FRL-PSII from *C. thermalis* (green points). Panel B in Fig. 8 shows the spectra for the three PSII preparations. The three spectra are identical to the difference spectra $Tyr_Z^{\bullet}Q_A^{\bullet -}$-*minus*-$Tyr_ZQ_A$ head-to-tail. This suggests that the electrostatic environment resulting from the formation of $Tyr_Z^{\bullet}Q_A^{\bullet -}$ occurs with kinetics slower than the formation of the state. The different kinetics in Panel A of Fig. 8 could represent another manifestation of a different rearrangement of the electrostatic environment in the species studied here.

Conclusion

The effects of $Tyr_D^{\bullet}$, $Tyr_Z^{\bullet}$, and $Q_A^{\bullet -}$ radical formation on the absorption spectrum in the Soret region were studied in Mn-depleted Photosystem II (PSII) at pH 8.6. Flash-induced difference spectra were recorded for several PSII samples from: *i*) *Thermosynechococcus vestitus* (formerly *T. elongatus*), *ii*) *Synechocystis* sp. PCC 6803, *iii*) *Chroococcidiopsis thermalis* PCC7203 grown under far-red light, and *iv*) *Acaryochloris marina*. While P_{D1} is clearly the species whose spectrum is blue-shifted by ~3 nm in the presence of $Q_A^{\bullet -}$, the spectra recorded from these different samples suggest that P_{D1}, P_{D2}, Chl_{D1}, Phe_{D1}, and Chl_{D2} are not the species whose absorption spectrum is modified by the formation of $Tyr_D^{\bullet}$ and $Tyr_Z^{\bullet}$. The conclusion for Phe_{D1} is drawn from the similarity of the $Tyr_Z^{\bullet}$-*minus*-Tyr_Z difference spectrum in PsbA3-PSII with E-130 and PsbA1/Y160F-PSII with Q-130, as shown in [42]. It is therefore proposed that other pigments, such as antenna Chl and/or Car near the reaction center, are involved. Additionally, it is shown that: *i*) there is no proton release into the bulk upon the oxidation of Tyr_D at pH 8.6, and *ii*) the rearrangement of the electrostatic environment of the pigments involved in the light-induced difference spectra in the samples

studied, upon the formation of $Tyr_D^{\bullet}$, $Tyr_Z^{\bullet}$, and $Q_A^{\bullet-}$, likely occurs differently from both kinetic and structural perspectives.

Legends

Figure 1:

Panel A shows the ΔI/I changes recorded at 432 nm in Mn-depleted PsbA3-PSII from *T. vestitus* at pH 8.6. The sample was dark-adapted for 3 to 4 hours to allow Tyr_D to be almost fully reduced. After the dark adaptation, 100 µM of PPBQ, dissolved in dimethyl sulfoxide, were added. Flash illumination was performed with 10 saturating flashes (spaced 2 s apart). The first weak detector laser flash was given 200 µs after each of the saturating actinic laser flashes. The second detector flash was given 10 ms after each of the actinic flashes. Then, 20 detector flashes (spaced 100 ms apart) were given after each of the 10 actinic flashes. The optical density (OD) of the sample was 1.75 at 673 nm (~25 µg Chl/ml). The pathlength of the cuvette was 2.5 mm.

Panel B shows the same data as in Panel A, with an expanded time scale for the first 4 actinic flashes. The vertical black arrow, 2 s after the first flash, corresponds to the Δ(ΔI/I) mainly originating from the formation of $Tyr_D^{\bullet}$ alone, since $Q_A^{\bullet-}$ and $Tyr_Z^{\bullet}$ (formed in centers with $Tyr_D^{\bullet}$ present) are no longer present 2 s after the flash. After the 4th flash, when $Tyr_D^{\bullet}$ has been formed in the majority of centers, the flash illumination induces the formation of the $Tyr_Z^{\bullet}Q_A^{\bullet-}$ state. The vertical red arrow shows the Δ(ΔI/I) between 200 µs and 10 ms and corresponds to the $Tyr_Z^{\bullet}Q_A^{\bullet-}$-*minus*-$Tyr_Z^{\bullet}Q_A$ difference. The vertical violet arrow shows the Δ(ΔI/I) between 200 µs and 2 s and corresponds to the $Tyr_Z^{\bullet}Q_A^{\bullet-}$-*minus*-$Tyr_ZQ_A$ difference. The vertical green arrow shows the Δ(ΔI/I) between 400 ms and 2 s and corresponds to the $Tyr_Z^{\bullet}$-minus-Tyr_Z difference. The vertical orange arrow shows the Δ(ΔI/I) between 200 µs and 10 ms after the 1st actinic flash and corresponds to the $Q_A^{\bullet-}$-*minus*-Q_A difference (in the presence of $Tyr_D^{\bullet}$). The Δ(ΔI/I) between 10 ms and 400 ms will be analyzed in Fig. 8.

Figure 2:

The experiment conducted at 432 nm with PsbA3-PSII from *T. vestitus*, as reported in Panel A of Fig. 1, was repeated for wavelengths between 401 nm and 457 nm. The different Δ(ΔI/I) values, defined in Panel B of Fig. 1, were plotted using the color code established in Panel B of Fig. 1. Except for the spectra corresponding to the first flash, the Δ(ΔI/I) values were averaged from the 6th to the 10th flash.

Figure 3:

Panel A shows the ΔI/I changes recorded at 432 nm in Mn-depleted, Tyr_D-less PSII from *T. vestitus* at pH 8.6, using the same protocol as described in Panel A of Fig. 1.

Panel B shows the ΔI/I measured as in Panel A, for wavelengths between 401 nm and 457 nm, and plotted using the color code defined in Panel B of Fig. 1. Except for the spectra corresponding to the first flash, the Δ(ΔI/I) values were averaged from the 6th to the 10th flash.

Figure 4:

ΔI/I changes recorded at 580 nm in the presence of thymol blue (black data points) with dark-adapted Tyr_D-less PSII from *T. vestitus* at pH 8.6. The first detector flash was given 20 µs after each actinic flash. Then, 20 detector flashes (spaced 100 ms apart) were given after each of the 10 actinic flashes. The continuous red curve corresponds to a second-degree polynomial fit. The blue trace represents the black trace *minu*s the red curve. This procedure was used to subtract as much drift as possible from the black trace.

Figure 5:

Panel A, spectra of the $Tyr_Z^{\bullet}Q_A^{\bullet-}$-*minus*-$Tyr_Z^{\bullet}Q_A$ difference in various PSII samples. Same conditions as in Panels A and B in Fig. 1.

Panel B, spectra of the $Tyr_Z^{\bullet}Q_A^{\bullet-}$-*minus*-$Tyr_ZQ_A$ difference in various PSII samples. Same conditions as in Panels A and B in Fig. 1.

Panel C, spectra of the $Tyr_Z^{\bullet}$-*minus*-Tyr_Z difference in various PSII samples. Same conditions as in Panels A and B in Fig. 1.

Panel D, spectra of the $Tyr_D^{\bullet}$-*minus*-Tyr_D difference in various PSII samples. Same conditions as in Panels A and B in Fig. 1.

All the spectra were normalized to -1 for the amplitude of the trough.

Figure 6:

Panel A, spectra of the $Tyr_Z^{\bullet}Q_A^{\bullet-}$-*minus*-$Tyr_Z^{\bullet}Q_A$ difference in wild type *Synechocystis* 6803 (black spectrum) and in the D2/H197A mutant (green spectrum). Same conditions as in Panels A and B in Fig. 1.

Panel B, spectra of the $Tyr_Z^{\bullet}Q_A^{\bullet-}$-*minus*-$Tyr_ZQ_A$ difference in wild type *Synechocystis* 6803 (black spectrum) and in the D2/H197A mutant (green spectrum). Same conditions as in Panels A and B in Fig. 1.

Panel C, spectra of the $Tyr_D^{\bullet}$-*minus*-Tyr_D difference in wild type *Synechocystis* 6803 (black spectrum) and in the D2/H197A mutant (green spectrum). Same conditions as in Panels A and B in Fig. 1.

Panel D, spectra of the $Tyr_Z^{\bullet}$-*minus*-Tyr_Z difference in wild type *Synechocystis* 6803 (black spectrum) and in the D2/H197A mutant (green spectrum). Same conditions as in Panels A and B in Fig. 1.

All the spectra were normalized to -1 for the amplitude of the trough.

Figure 7:

Panel A, spectra of the $Tyr_D^{\bullet}$-*minus*-Tyr_D difference at pH 6.5 in *C. thermalis* (black spectrum) and in PSII from *A. marina* (red spectrum). Other conditions same as in Panels A and B in Fig. 1.

Panel B, spectra of the $Tyr_Z^{\bullet}$-*minus*-Tyr_Z difference at pH 6.5 in FRL-PSII from *C thermalis* (black spectrum) and in PSII from *A. marina* (red spectrum). Other conditions same as in Panels A and B in Fig. 1. The ΔI/I were averaged from the 6th to 10th flash.

Figure 8:

Panel A shows ΔI/I recorded at 432 nm and at pH 8.6 in Mn-depleted PSII from *C. thermalis* (green data points), from *T. vestitus* (black data points), and from the D1/H198Q mutant in *T. vestitus* (red data points). The ΔI/I values were averaged from the 6th to the 10th flash. The first point corresponds to the detector flash given 10 ms after the actinic flash.

Panel B shows the wavelength dependence of the maximum amplitude of the kinetics from Panel A, measured at 300 ms for PsbA3-PSII from *T. vestitus*, at 100 ms for FRL-PSII from *C. thermalis*, and at 500 ms for D1/H198Q PSII from *T. vestitus*.

References

[1] Y. Umena, K. Kawakami, J.-R. Shen, N. Kamiya, Crystal structure of oxygen evolving Photosystem II at a resolution of 1.9 angstrom, Nature 473 (2011) 55–60, https://doi.org/10.1038/nature09913

[2] H. Ago, H. Adachi, Y. Umena, T. Tashiro, K. Kawakami, N. Kamiya, L.R. Tian, G.Y. Han, T.Y. Kuang, Z.Y. Liu, F.J. Wang, H.F. Zou, I. Enami, M. Miyano, J.-R. Shen, Novel features of eukaryotic photosystem II revealed by its crystal structure analysis from a red alga, J. Biol. Chem. 291 (2016) 5676–5687, https://doi.org/10.1074/jbc.M115.711689

[3] C.J. Gisriel, J. Wang, J. Liu, D.A. Flesher, K.M. Reiss, H.-L. Huang, K.R. Yang, W.H. Armstrong, M.R. Gunner, V.S. Batista, R.J. Debus, G.W. Brudvig, High resolution cryo-electron microscopy structure of photosystem II from the mesophilic cyanobacterium, *Synechocystis* sp. PCC 6803, Proc. Natl. Acad. Sci. U. S. A. 119 (2022), e2116765118, https://doi.org/10.1073/pnas.2116765118

[5] A.R. Holzwarth, M.G. Müller, M. Reus, M. Nowaczyk, J. Sander, M. Rögner, Kinetics and mechanism of electron transfer in intact Photosystem II and in the isolated reaction center: pheophytin is the primary electron acceptor, Proc. Natl. Acad. Sci. U. S. A. 103 (2006) 6895–6900, https://doi.org/10.1073/pnas.0505371103

[6] F. Muh, M. Plockinger, T. Renger, Electrostatic asymmetry in the reaction center of Photosystem II, J. Phys. Chem. Lett. 8 (2017) 850–858, https://doi.org/10.1021/acs.jpclett.6b02823

[7] A. Sirohiwal, D.A. Pantazis, Reaction center excitation in Photosystem II: From multiscale modeling to functional principles, Acc. Chem. Res. (2023) 2921−2932. https://doi.org/10.1021/acs.accounts.3c00392

[8] D.J. Vinyard, G.M. Ananyev, G.C. Dismukes, Photosystem II: the reaction center of oxygenic photosynthesis, Annu. Rev. Biochem. 82 (2013) 577–606. https://10.1146/annurev-biochem-070511-100425

[9] D. Shevela J.F. Kern G. Govindjee J. Messinger , Solar energy conversion by photosystem II: principles and structures, Photosynth. Res. 156 (2023) 279–307. https://doi.org/10.1007/s11120-022-00991-y

[10] W. Lubitz D.A. Pantazis N. Cox , Water oxidation in oxygenic photosynthesis studied by magnetic resonance techniques, FEBS Lett. 597 (2023) 6–29. https://doi.org/10.1002/1873-3468.14543

[11] N. Oliver, A.P. Avramov, D.J. Nürnberg, H. Dau, R.L. Burnap, From manganese oxidation to water oxidation: assembly and evolution of the water-splitting complex in photosystem II, Photosynth. Res. 152 (2022) 107–133, https://doi.org/10.1007/s11120-022-00912-z

[12] T. Oliver, T.D. Kim, J.P. Trinugroho, V. Cord´on-Preciado, N. Wijayatilake, A. Bhatia, A.W. Rutherford, T. Cardona, The evolution and evolvability of photosystem II, Annu. Rev. Plant Biol. 74 (2023) 24.1–24.33, https://doi.org/10.1146/annurev-arplant-070522-062509

[13] P. Joliot, Period-four oscillations of the flash-induced oxygen formation in photosynthesis, Photosynth. Res. 76 (2003) 65–72. https://doi.org/10.1023/A:1024946610564

[14] B. Kok, B. Forbush, M. McGloin, Cooperation of charges in photosynthetic O_2 evolution–I. A linear four step mechanism, Photochem. Photobiol. 11 (1970) 457–475, https://doi.org/10.1111/j.1751-1097.1970.tb06017.x

[15] E.J. Bylina, C. Kirmaier, L. McDowell, D. Holten, D.C. Youvan, Influence of an amino-acid residue on the optical properties and electron transfer dynamics of a photosynthetic reaction center complex, Nature 336 (1988) 182–184. https://doi.org/10.1038/336182a0

[16] D.H. Stewart, P.J. Nixon, B.A. Diner, G.W. Brudvig, Assignment of the Qy absorbance bands of photosystem II chromophores by low-temperature optical spectroscopy of wild-type and mutant reaction centres, Biochemistry 39 (2000) 14583–14594. https://doi.org/10.1021/bi001246j

[17] L.B. Giorgi, P.J. Nixon, S.A.P. Merry, D.M. Joseph, J.R. Durrant, J.D. Rivas, J. Barber, G. Porter, D.R. Klug, Comparison of primary charge separation in the photosystem II reaction center complex isolated from wild-type and D1–130 mutants of the cyanobacterium Synechocystis PCC 6803, J. Biol. Chem. 271 (1996) 2093–2101. https://doi.org/10.1074/jbc.271.4.2093

[18] B.A. Diner, E. Schlodder, P.J. Nixon, W.J. Coleman, F. Rappaport, J. Lavergne, W.F. J. Vermaas, D.A. Chisholm, Site-directed mutations at D1-His198 and D2-His197 of photosystem II in *Synechocystis* PCC 6803: sites of primary charge separation and cation and triplet stabilization, Biochemistry 24 (2001) 9265–9281. https://doi.org/10.1021/bi010121r

[19] E. Schlodder, W.J. Coleman, P.J. Nixon, R.O. Cohen, T. Renger, B.A. Diner, Site directed mutations at D1-His198 and D1-Thr179 of photosystem II in *Synechocystis* sp. PCC 6803: deciphering the spectral properties of the PSII reaction centre, Philos. Trans. R. Soc. B 363 (2008) 1197−1202. https://doi.org/10.1098/rstb.2007.2215

[20] D.J. Nürnberg, J. Morton, S. Santabarbara, A. Telfer, P. Joliot, L.A. Antonaru, A. H. Ruban, T. Cardona, E. Krausz, A. Boussac, A. Fantuzzi, A.W. Rutherford, Photochemistry

beyond the red-limit in the chlorophyll f-containing photosystems, Science 360 (2018) 1210–1213. https://doi.org/10.1126/science.aar8313

[21] F. Rappaport, M. Blanchard-Desce, J. Lavergne, Kinetics of electron-transfer and electrochromic change during the redox transitions of the photosynthetic oxygen evolving complex, Biochim. Biophys. Acta 1184 (1994) 178–192. https://doi.org/10.1016/0005-2728(94)90222-4

[22] F. Rappaport, J. Lavergne, Proton release during successive oxidation steps of the photosynthetic water oxidation process: stoichiometries and pH dependence, Biochemistry 30 (1991) 10004–10012. https://doi.org/10.1021/bi00105a027

[23] P. Faller, R.J. Debus, K. Brettel, M. Sugiura, A.W. Rutherford, A. Boussac, Rapid formation of the stable tyrosyl radical in photosystem II, Proc Natl Acad Sci USA 98 (2001)14368–14373. https://doi.org/10.1073/pnas.251382598

[24] M. Sugiura, A. Boussac, T. Noguchi, F. Rappaport, Influence of Histidine-198 of the D1 subunit on the properties of the primary electron donor, P680, of photosystem II in *Thermosynechococcus elongatus*, Biochim. Biophys. Acta 1777 (2008) 331–342, https://doi.org/10.1016/j.bbabio.2008.01.007

[25] M. Sugiura, Y. Osaki, F. Rappaport, A. Boussac, Corrigendum to "Influence of Histidine-198 of the D1 subunit on the properties of the primary electron donor, P680, of Photosystem II in *Thermosynechococcus elongatus*". Biochim. Biophys. Acta 1857 (2016)1943–1948. https://doi.org/10.1016/j.bbabio.2016.09.012

[26] Y. Takegawa, M. Nakamura, S. Nakamura, T. Noguchi, J. Sellés, A.W. Rutherford, A. Boussac, M. Sugiura, New insights on Chl_{D1} function in photosystem II from site-directed mutants of D1/T179 in *Thermosynechococcus elongatus*, Biochim. Biophys. Acta 1860 (2019) 297–309. https://doi.org/10.1016/j.bbabio.2019.01.008

[27] M. Sugiura, F. Rappaport, K. Brettel, T. Noguchi, A.W. Rutherford, A. Boussac , Site-directed mutagenesis of the *Thermosynechococcus elongatus* photosystem II: the O_2-evolving enzyme lacking the redox-active tyrosine D, Biochemistry 43 (2004) 13549–13563. https://doi.org/10.1021/bi048732h

[28] M. Sugiura, M. Kimura, N. Shimamoto, Y. Takegawa, M. Nakamura, K. Koyama, J. Sellés, A. Boussac, A.W. Rutherford, Tuning of the Chl_{D1} and Chl_{D2} properties in photosystem II by site-directed mutagenesis of neighbouring amino acids, Biochim. Biophys. Acta 1865 (2024) 149013. https://doi.org/10.1016/j.bbabio.2023.149013

[29] S. Viola, W. Roseby, S. Santabarabara, D. Nürnberg, R. Assunção, H. Dau, J. Sellés, A. Boussac, A. Fantuzzi, A.W. Rutherford, Impact of energy limitations on function and

resilience in long-wavelength Photosystem II, eLife 11 (2022) e79890. https://doi.org/10.1101/2022.04.05.486971

[30] T. Hayase, Y. Shimada, T. Mitomi, R. Nagao, T. Noguchi, Triplet delocalization over the reaction center chlorophylls in Photosystem II. J Phys Chem 127 (2023) 1758–1770. https://doi.org/10.1021/acs.jpcb.3c00139

[31] T. Renger, E. Schlodder, The primary electron donor of photosystem II of the cyanobacterium *Acaryochloris marina* is a chlorophyll d and the water oxidation is driven by a chlorophyll a/chlorophyll d heterodimer, J. Phys. Chem. B 112 (2008)7351–7354. https://doi.org/10.1021/jp801900e

[32] D. Béal, F. Rappaport, P. Joliot, A new high-sensitivity 10-ns time-resolution spectrophotometric technique adapted to in vivo analysis of the photosynthetic apparatus, Rev. Sci. Instrum. 70 (1999) 202–207. https://doi.org/10.1063/1.1149566

[33] M. Sugiura, T. Taniguchi, N. Tango, M. Nakamura, J. Sellés, A. Boussac, Probing the role of arginine 323 of the D1 protein in photosystem II function, Physiol. Plant. 171 (2021) 183–199. https://doi.org/10.1111/ppl.13115

[34] B.A. Diner, V. Petrouleas, Q400, the non-heme iron of the Photosystem-II iron-quinone complex – a spectroscopic proble of quinone and inhibitor binding to the reaction center, Biochim. Biophys. Acta 895 (1987) 107–125. https://doi.org/10.1016/S0304-4173(87)80010-1

[35] A. Boussac, M. Sugiura, F. Rappaport, Probing the quinone binding site of photosystem II from Thermosynechococcus elongatus containing either PsbA1 or PsbA3 as the D1 protein through the binding characteristics of herbicides, Biochim. Biophys. Acta 1807 (2010) 119–129, https://doi.org/10.1016/j.bbabio.2010.10.004

[36] A. Boussac, M. Sugiura, M. Nakamura, R. Nagao, T. Noguchi, S. Viola, A. W. Rutherford, J. Sellés, Photosynth. Res. (2023). https://doi.org/10.1007/s11120-023-01049-3

[37] H. Conjeaud, P. Mathis, The effect of pH on the reduction kinetics of P-680 in tris-treated chloroplasts, Biochim. Biophys. Acta 590 (1980) 353–359. https://doi.org/10.1016/0005-2728(80)90206-6

[38] R. de Wijn, H.J. van Gorkom, Kinetics of electron transfer from Q_A to Q_B in Photosystem II, Biochemistry 40 (2001) 11912–1192210. https://doi.org/1021/bi010852r

[39] R. Hienerwadel, S. Gourion-Arsiquaud, M. Ballottari, R. Bassi, B.A. Diner, C. Berthomieu, Formate binding near the redox-active TyrosineD in Photosystem II:

consequences on the properties of Tyr_D, Photosynth. Res. 84 (2005) 139–144. https://doi.org/10.1007/s11120-005-0637-x

[40] S. Nakamura, T. Noguchi, Infrared detection of a proton released from tyrosine Y_D to the bulk upon its photo-oxidation in Photosystem II, Biochemistry 54 (2015) 5045–5053. https://doi.org/10.1021/acs.biochem.5b00568

[41] A. Boussac, J. Sellés, M. Sugiura, What can we still learn from the electrochromic band-shifts in photosystem II? Biochim. Biophys. Acta 2020 (1861) 148176, https://doi.org/10.1016/j.bbabio.2020.148176.

[42] M. Sugiura, C. Azami, K. Koyama, A.W. Rutherford, F. Rappaport, A. Boussac, Modification of the pheophytin redox potential in *Thermosynechococcus elongatus* Photosystem II with PsbA3 as D1, Biochim. Biophys. Acta 1837 (2014) 139–148. https://doi.org/10.1016/j.bbabio.2013.09.009

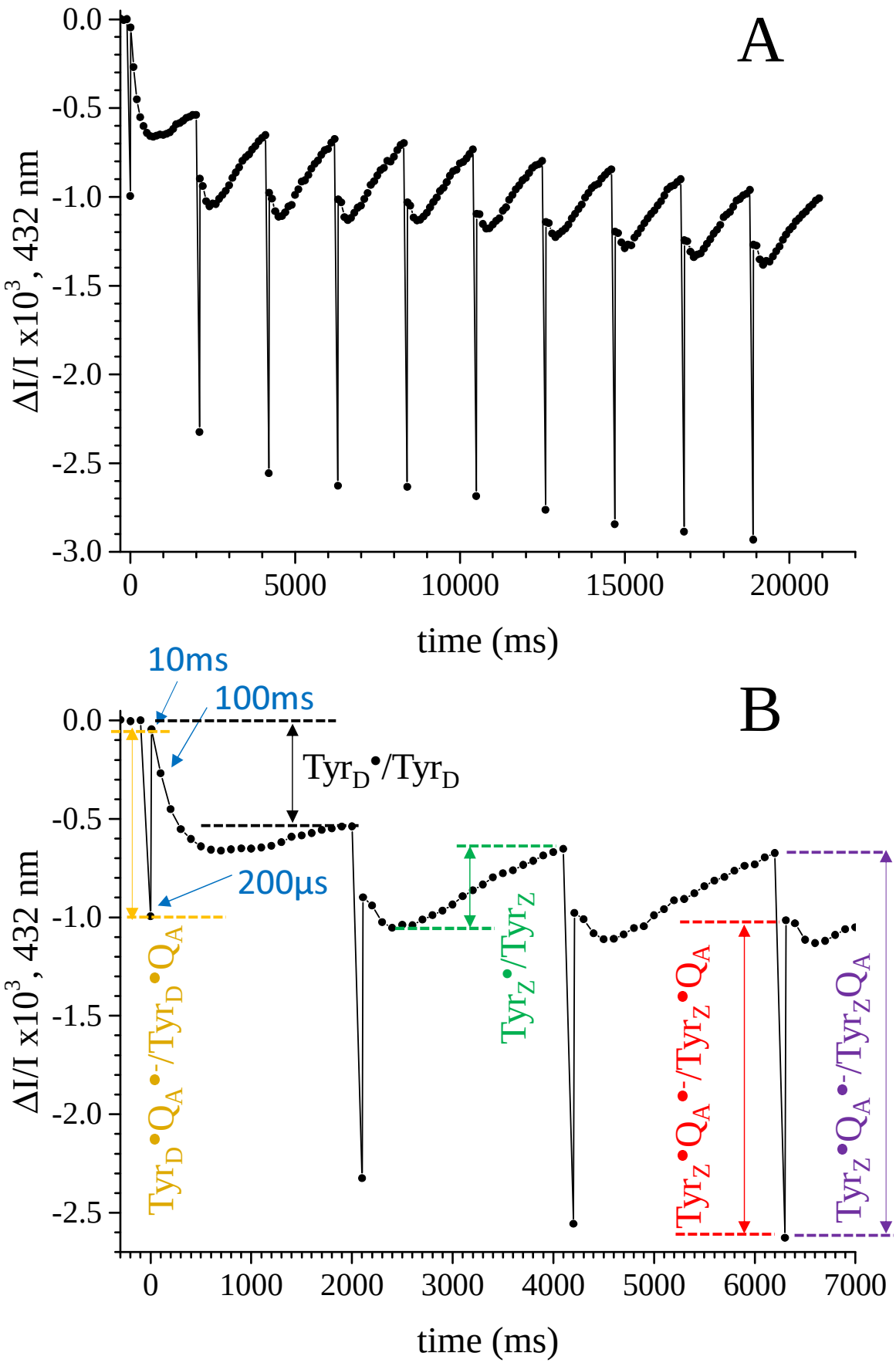
A
0.0
-0.5
-1.0
-1.5
-2.0
-2.5
-3.0
ΔI/I x10^3, 432 nm
0
5000
10000
15000
20000
time (ms)
B
10ms
100ms
200µs
Tyr_D•/Tyr_D
Tyr_D•Q_A•-/Tyr_D•Q_A
Tyr_Z•/Tyr_Z
Tyr_Z•Q_A•-/Tyr_Z•Q_A
Tyr_Z•Q_A•-/$Tyr_Z$$Q_A$
0.0
-0.5
-1.0
-1.5
-2.0
-2.5
ΔI/I x10^3, 432 nm
0
1000
2000
3000
4000
5000
6000
7000
time (ms)

Fig. 1

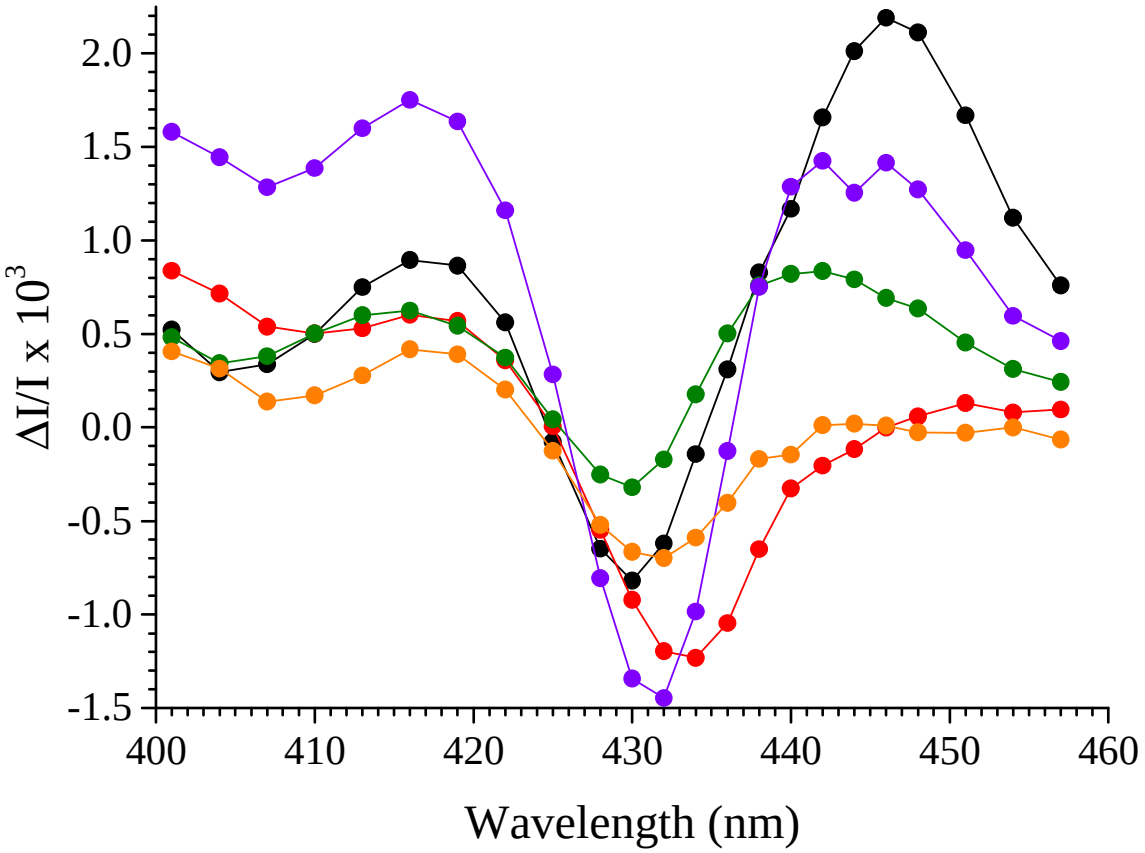
2.0
1.5
1.0
0.5
0.0
-0.5
-1.0
-1.5
ΔI/I x 10^3
400
410
420
430
440
450
460
Wavelength (nm)

Fig. 2

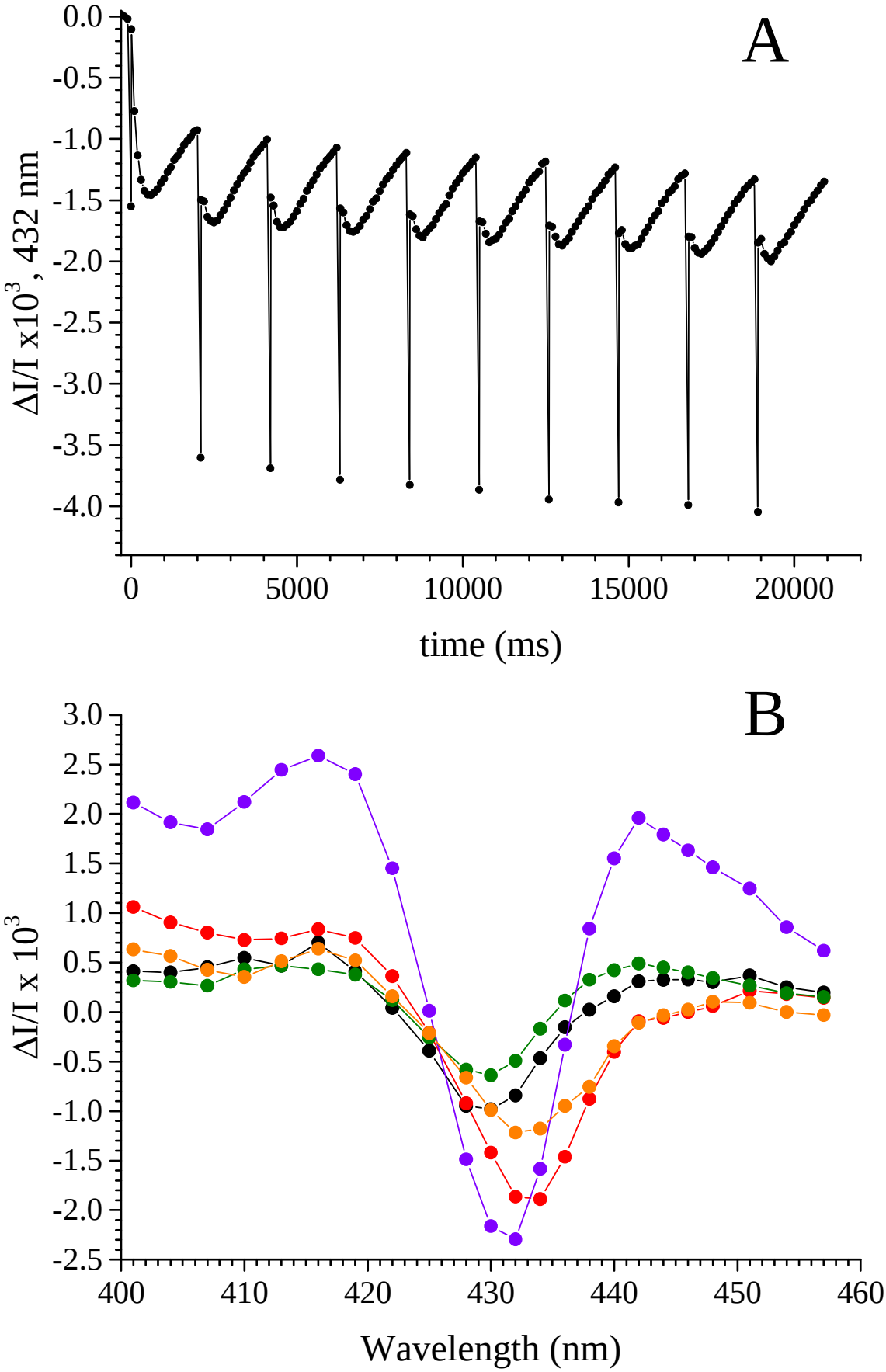
A
0.0
-0.5
-1.0
-1.5
-2.0
-2.5
-3.0
-3.5
-4.0
ΔI/I x10^3, 432 nm
0
5000
10000
15000
20000
time (ms)
B
3.0
2.5
2.0
1.5
1.0
0.5
0.0
-0.5
-1.0
-1.5
-2.0
-2.5
ΔI/I x 10^3
400
410
420
430
440
450
460
Wavelength (nm)

Fig. 3

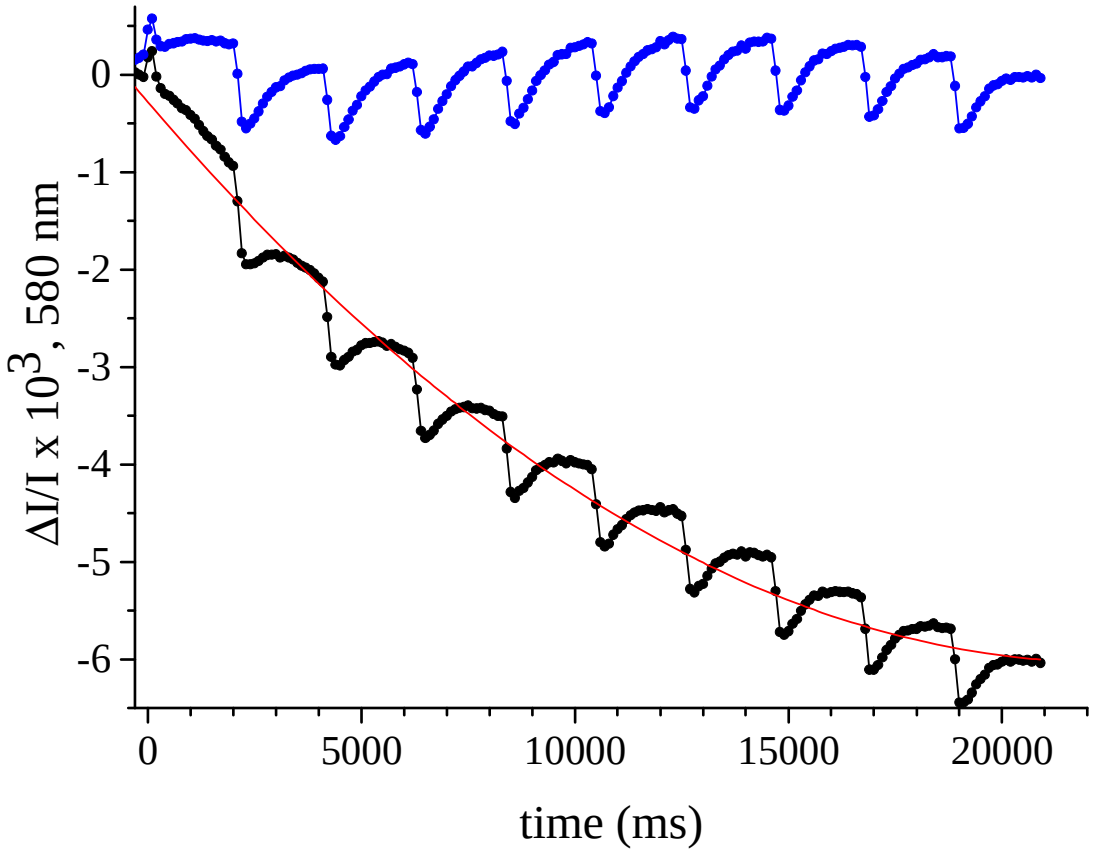

Fig. 4

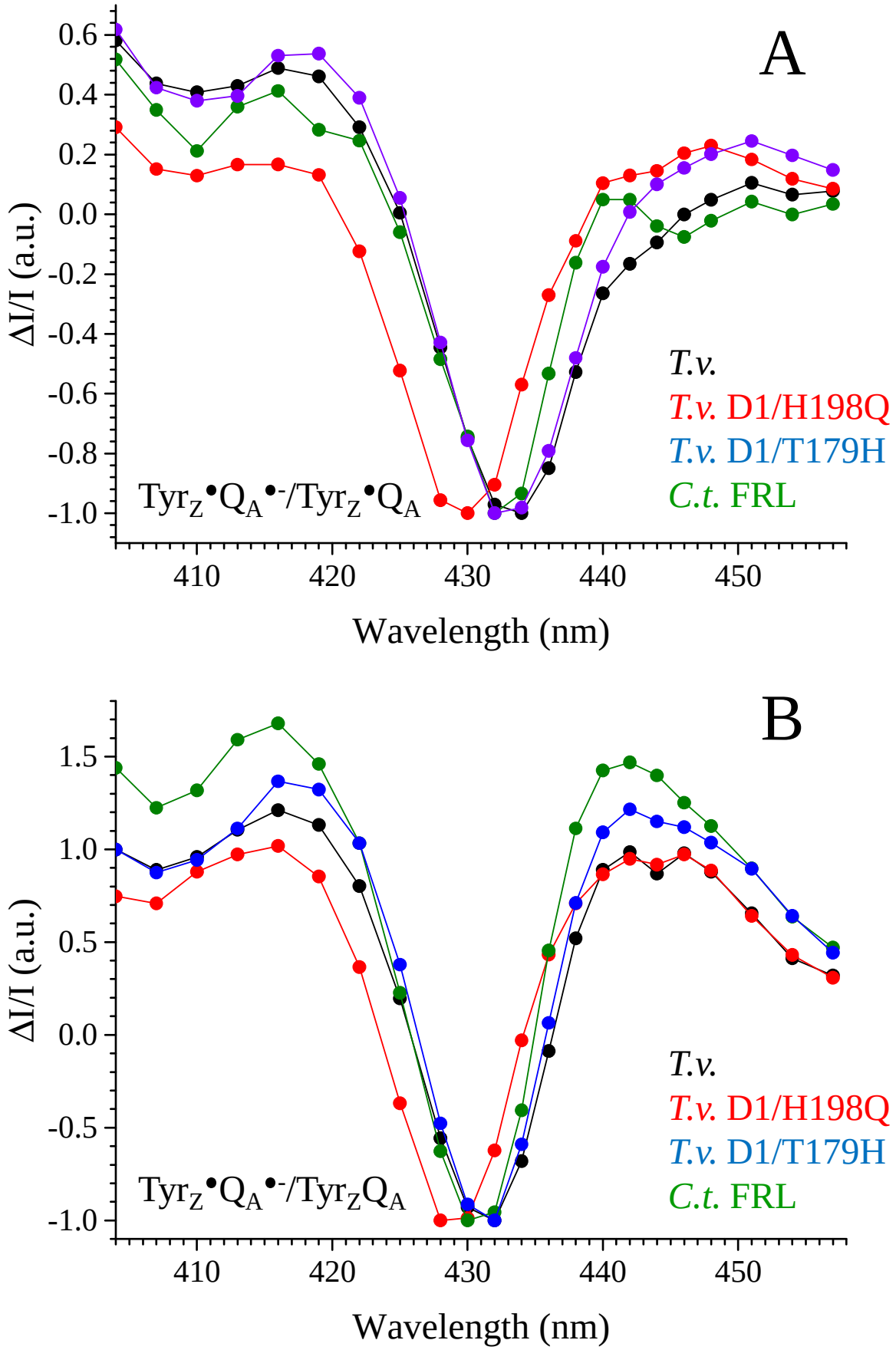
A
0.6
0.4
0.2
0.0
-0.2
-0.4
-0.6
-0.8
-1.0
ΔI/I (a.u.)
410
420
430
440
450
Wavelength (nm)
Tyr$_Z$•Q$_A$•$^-$/Tyr$_Z$•Q$_A$
T.v.
T.v. D1/H198Q
T.v. D1/T179H
C.t. FRL
B
1.5
1.0
0.5
0.0
-0.5
-1.0
ΔI/I (a.u.)
410
420
430
440
450
Wavelength (nm)
Tyr$_Z$•Q$_A$•$^-$/Tyr$_Z$Q$_A$
T.v.
T.v. D1/H198Q
T.v. D1/T179H
C.t. FRL

Fig. 5

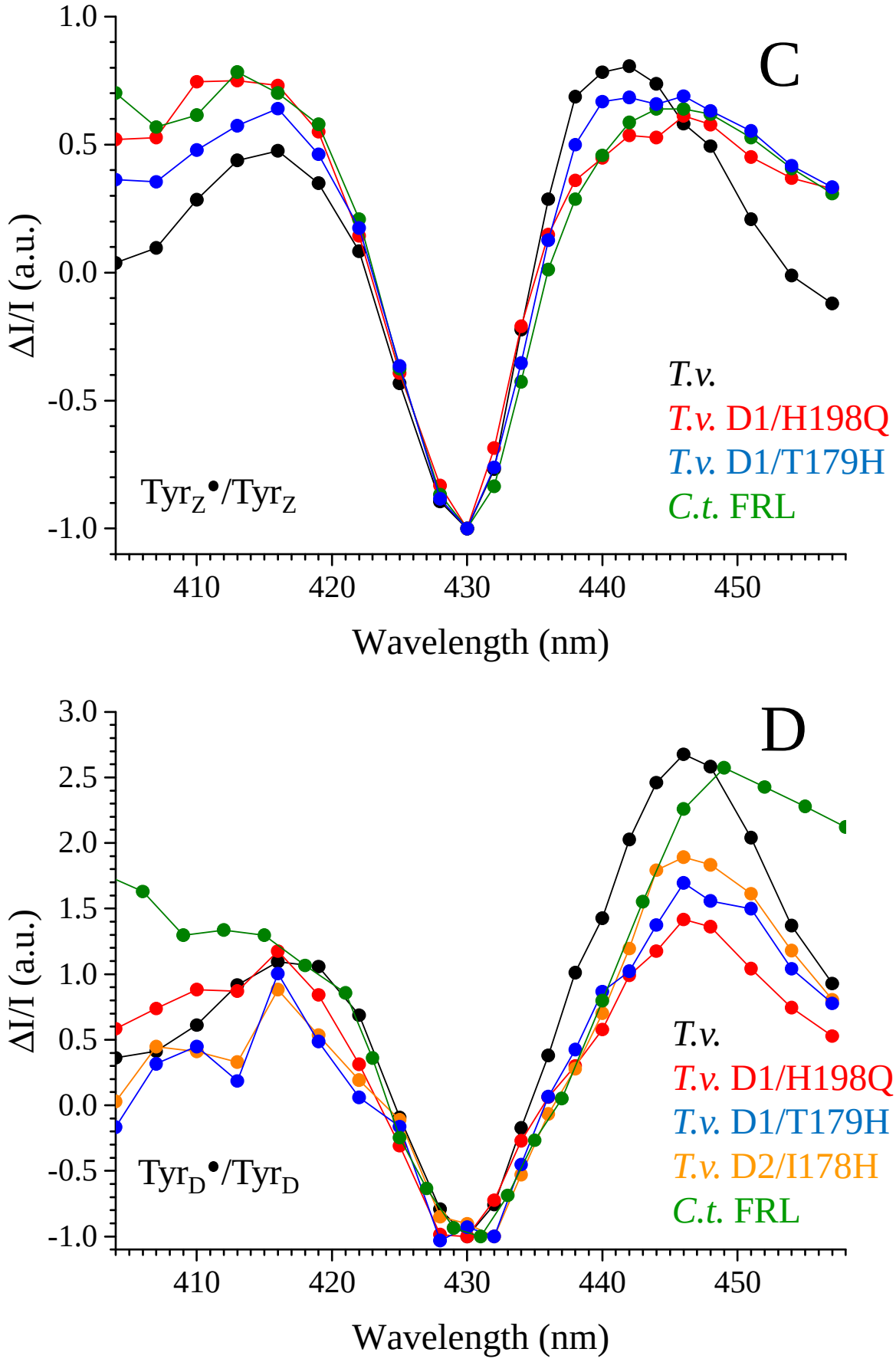
C
1.0
0.5
0.0
-0.5
-1.0
ΔI/I (a.u.)
410
420
430
440
450
Wavelength (nm)
Tyr$_Z$•/Tyr$_Z$
T.v.
T.v. D1/H198Q
T.v. D1/T179H
C.t. FRL
D
3.0
2.5
2.0
1.5
1.0
0.5
0.0
-0.5
-1.0
ΔI/I (a.u.)
410
420
430
440
450
Wavelength (nm)
Tyr$_D$•/Tyr$_D$
T.v.
T.v. D1/H198Q
T.v. D1/T179H
T.v. D2/I178H
C.t. FRL

Fig. 5

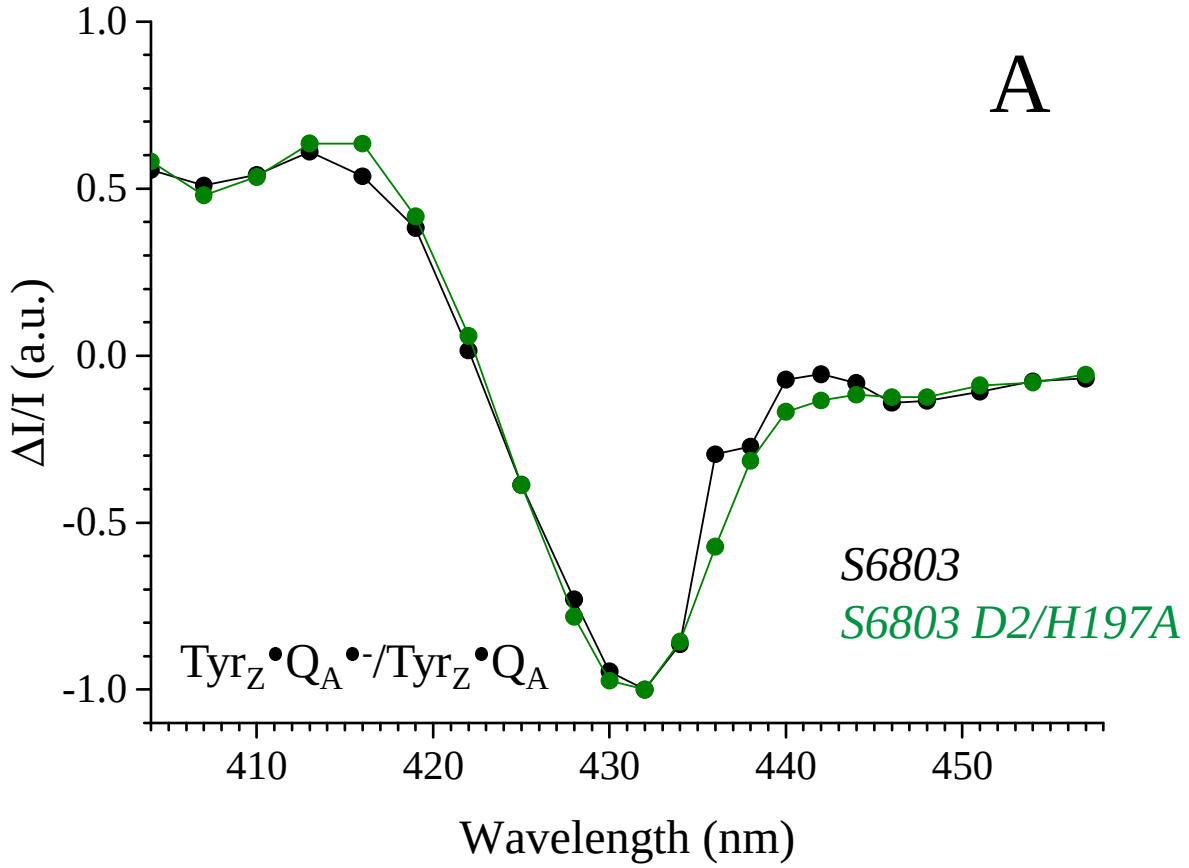
A
1.0
0.5
0.0
-0.5
-1.0
ΔI/I (a.u.)
410
420
430
440
450
Wavelength (nm)
S6803
S6803 D2/H197A
TyrZ•QA•-/TyrZ•QA

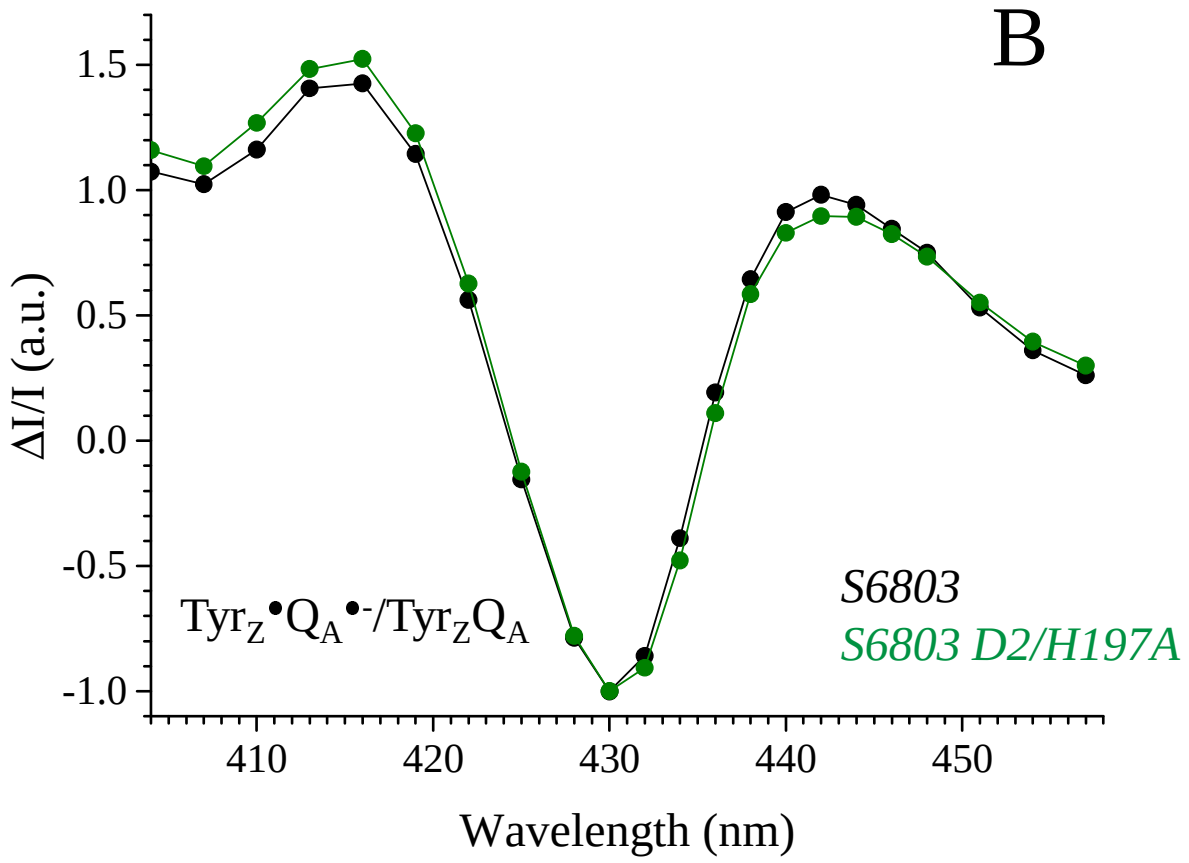
B
1.5
1.0
0.5
0.0
-0.5
-1.0
ΔI/I (a.u.)
410
420
430
440
450
Wavelength (nm)
S6803
S6803 D2/H197A
TyrZ•QA•-/TyrZQA

Fig. 6

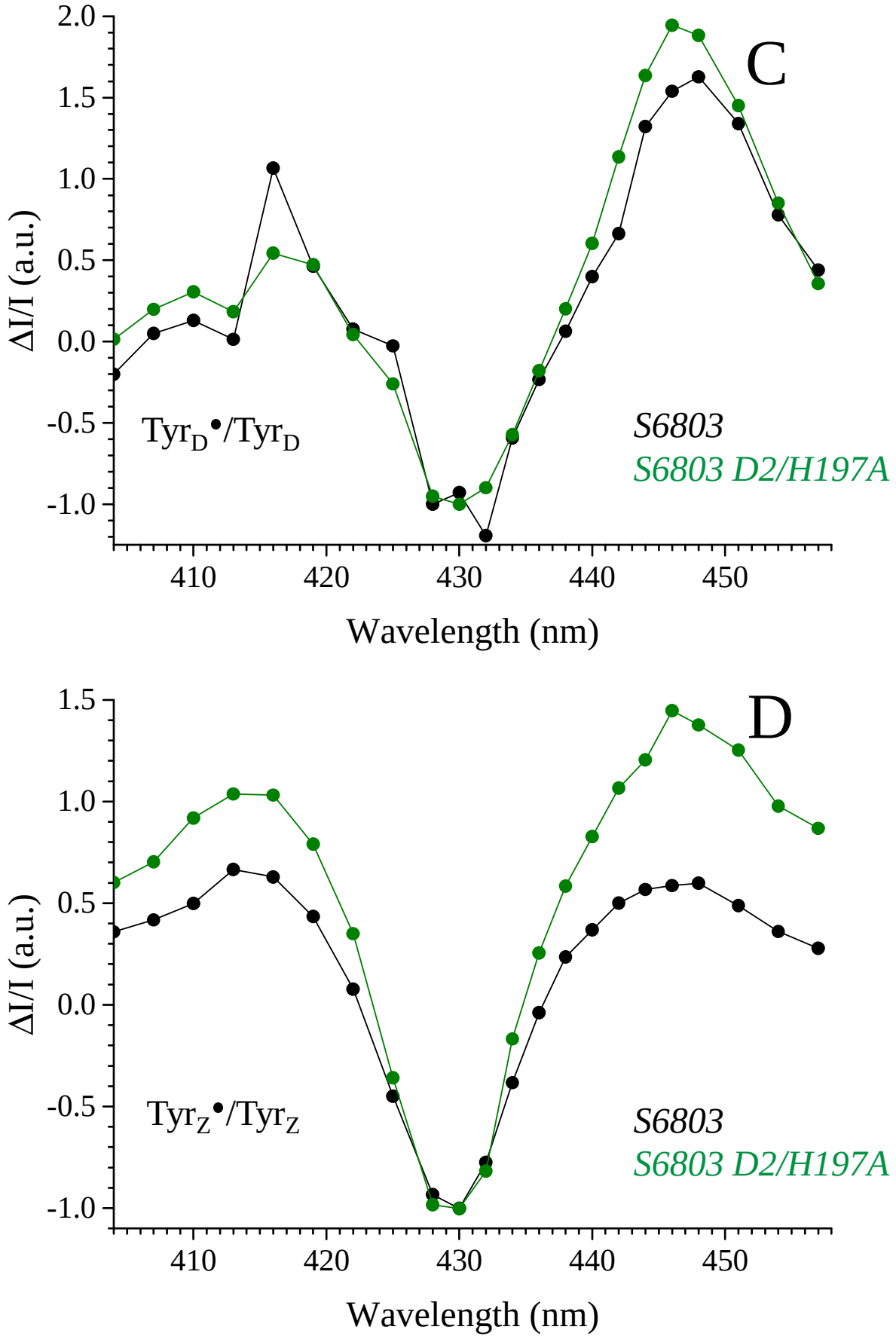
C
2.0
1.5
1.0
0.5
0.0
-0.5
-1.0
ΔI/I (a.u.)
Tyr$_D$•/Tyr$_D$
S6803
S6803 D2/H197A
410
420
430
440
450
Wavelength (nm)
D
1.5
1.0
0.5
0.0
-0.5
-1.0
ΔI/I (a.u.)
Tyr$_Z$•/Tyr$_Z$
S6803
S6803 D2/H197A
410
420
430
440
450
Wavelength (nm)

Fig. 6

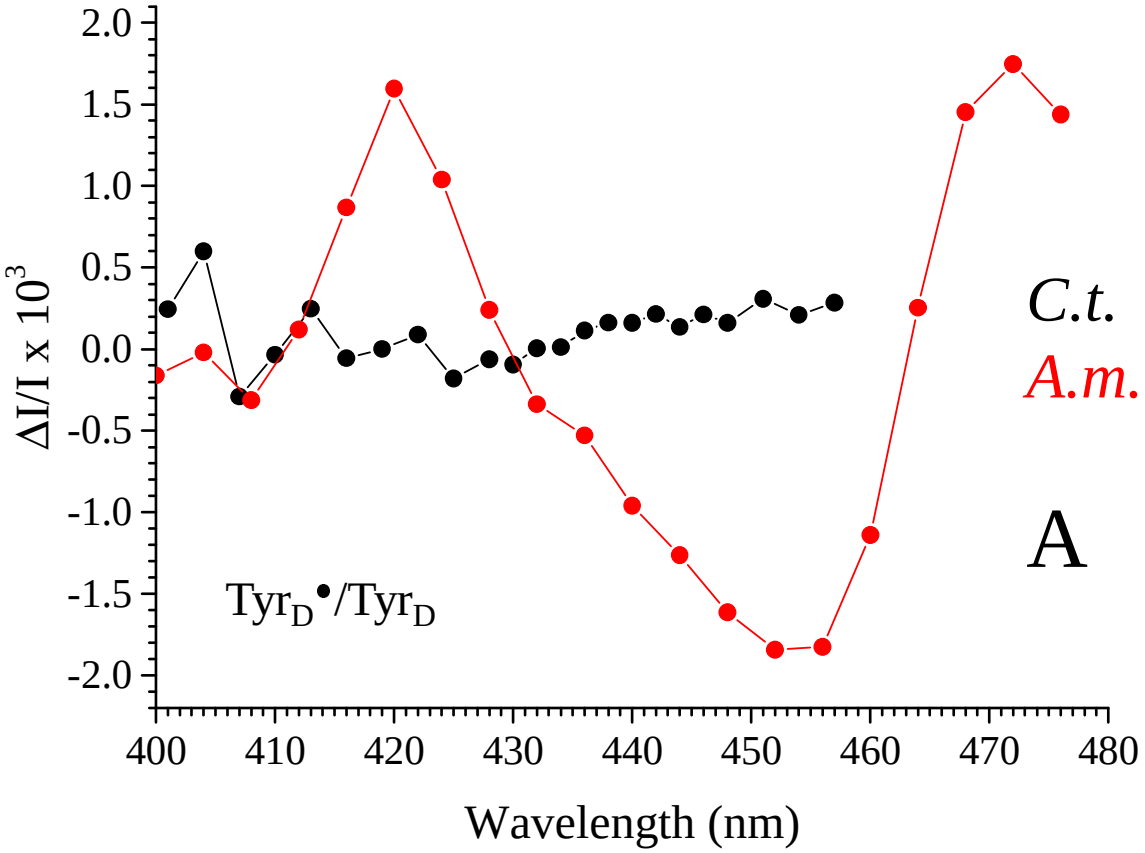
2.0
1.5
1.0
0.5
0.0
-0.5
-1.0
-1.5
-2.0
ΔI/I x 10^3
400
410
420
430
440
450
460
470
480
Wavelength (nm)
C.t.
A.m.
A
Tyr_D•/Tyr_D

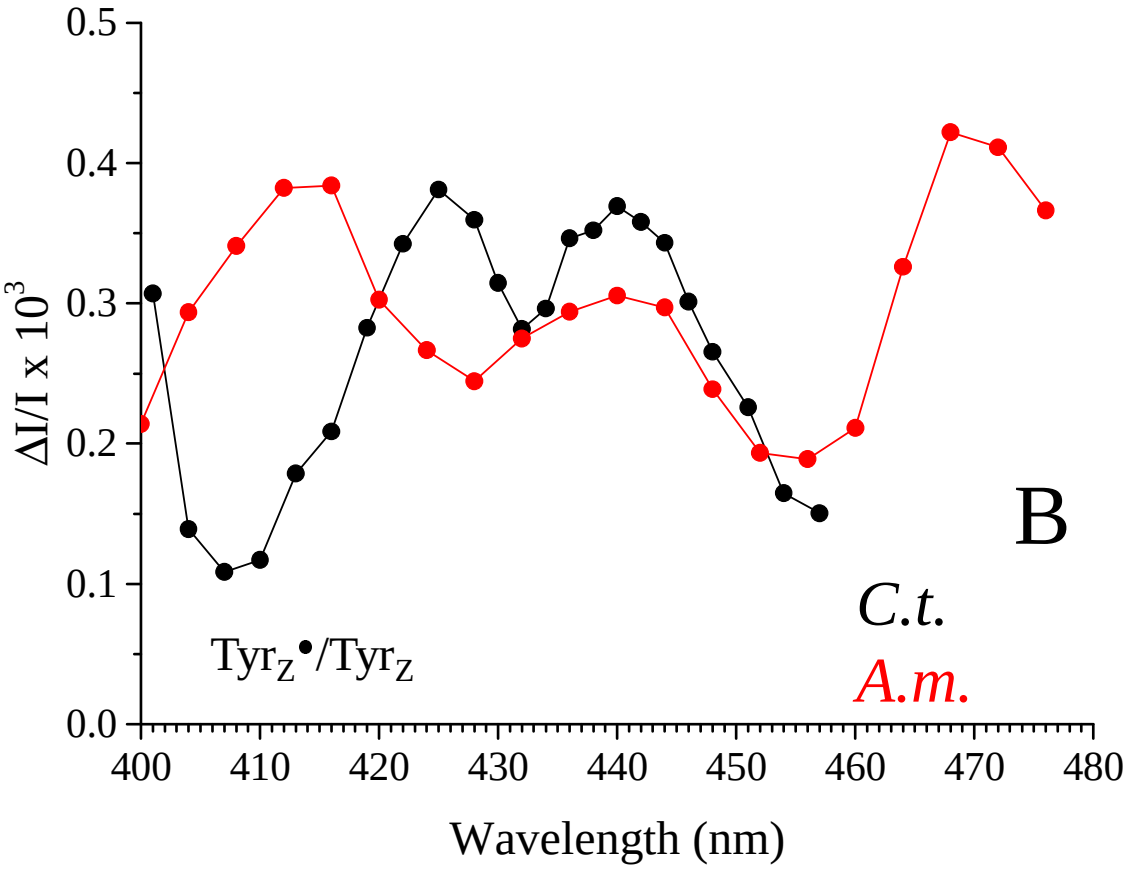
0.5
0.4
0.3
0.2
0.1
0.0
ΔI/I x 10^3
400
410
420
430
440
450
460
470
480
Wavelength (nm)
B
C.t.
A.m.
Tyr_Z•/Tyr_Z

Fig. 7

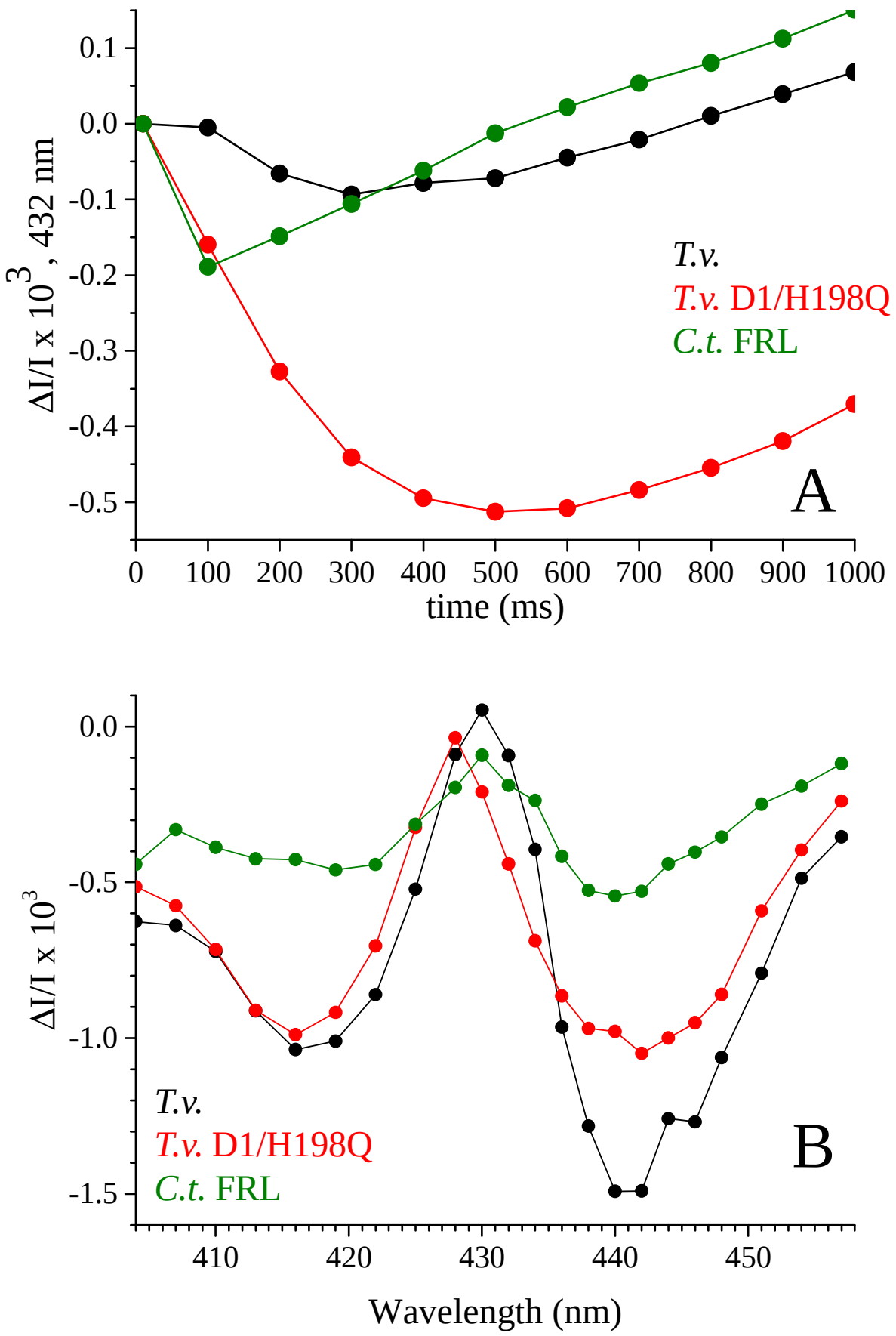
0.1
0.0
-0.1
-0.2
-0.3
-0.4
-0.5
ΔI/I x 10^3, 432 nm
0
100
200
300
400
500
600
700
800
900
1000
time (ms)
T.v.
T.v. D1/H198Q
C.t. FRL
A
0.0
-0.5
-1.0
-1.5
ΔI/I x 10^3
410
420
430
440
450
Wavelength (nm)
T.v.
T.v. D1/H198Q
C.t. FRL
B

Fig. 8